J. Fluid Mech. (2025), *vol.* 1007, A31, doi:10.1017/jfm.2025.61

Influence of irregular three-dimensional rough surfaces on the roughness function

Pietro Scandura

Department of Civil Engineering and Architecture, University of Catania, Via Santa Sofia 64, 95123 Catania, Italy

Corresponding author: Pietro Scandura, pietro.scandura@unict.it

(Received 17 May 2024; revised 5 December 2024; accepted 7 January 2025)

The influence of irregular three-dimensional rough surfaces on the displacement of the logarithmic velocity profile relative to that of a smooth wall in turbulent flow, known as the roughness function, is studied using direct numerical simulations. Five different surface power spectral density (PSD) shapes were considered, and for each, several rough Gaussian surfaces were generated by varying the root mean square (k_{rms}) of the surface heights. It is shown that the roughness function (ΔU^+) depends on both the PSD and k_{rms}. For a given k_{rms}, ΔU^+ increases as the wavenumbers of the PSD expand to large values, but at a rate that decreases with the magnitude of the wavenumbers. Although ΔU^+ generally does not scale with either k_{rms} or the effective slope ES when these variables are considered singularly, for PSDs with low wavenumbers, ΔU^+ tends to scale with ES, whereas as wavenumbers increase, ΔU^+ tends to scale with k_{rms}. An equivalent Nikuradse sand roughness of about eight times k_{rms} is found, which is similar to that observed in previous studies for a regular three-dimensional roughness. Finally, it is shown that k_{rms} and the effective slope are sufficient to describe the roughness function in the transitional rough regime.

Key words: turbulence simulation

1. Introduction

Flow near rigid boundaries is often affected by surface roughness and this has stimulated numerous studies aimed at quantifying the effect of roughness geometry on flow. However, these studies are still inconclusive as the multiple scales involved make it difficult to identify the most important geometric roughness parameters. The influence of rough

© The Author(s), 2025. Published by Cambridge University Press. This is an Open Access article, distributed under the terms of the Creative Commons Attribution licence (https://creativecommons.org/licenses/by/4.0/), which permits unrestricted re-use, distribution and reproduction, provided the original article is properly cited.

https://doi.org/10.1017/jfm.2025.61 Published online by Cambridge University Press

surfaces on the friction exerted by fluids is of interest in a wide variety of fields, including turbomachinery, river flows, meteorological applications and many others. The reader is referred to Jiménez (2004) and Chung *et al.* (2021) for thorough reviews of the subject. The first systematic experimental study in this field was carried out by Nikuradse (1933), who, in order to use an easily measurable roughness, glued sand of constant diameter to the inside wall of smooth pipes, so that a single length (the grain diameter) was suitable for describing the roughness size. Sand roughness size is now widely used as a measure of surface roughness. For ordinary pipes, roughness has a complex shape that cannot be described by a single length. Nevertheless, for these cases an equivalent sand roughness height (k_s) is used, which is defined as the diameter of the Nikuradse pipe sand grain that produces the same friction factor as the pipe under consideration in the fully rough turbulent regime. A weakness of this approach is that there is no guarantee that the matching of friction factors in the fully rough regime also provides a good match in the transitional rough regime.

The approach of Nikuradse (1933) to describe surface roughness belongs to the discrete approach (Stewart *et al.* 2019), where surface roughness is described by a set of linear scales, and although it has proven useful in several engineering applications, it is not entirely satisfactory for a detailed description of the complexity of a rough surface, as a large number of parameters should be considered, such as particle shape, orientation and degree of exposure. However, this is the approach generally used to describe river bed roughness. For example, van Rijn (1982) reported that the equivalent sand grain roughness k_s is related to D_{90} (90 % of the sample volume is made up of all particles with a diameter smaller than D_{90}), whereas Whiting & Dietrich (1990) assumed that k_s is proportional to D_{84}.

Another way of describing surface roughness is based on the continuous approach, where the roughness is considered as a random field of surface elevations (Nikora, Goring & Biggs 1998; Stewart *et al.* 2019) described by the moments of the frequency distribution and by the power spectral density (PSD). The choice between discrete and continuous approaches mainly concerns rough surfaces formed by granular elements, as in the case of river beds, whereas in industrial applications the continuous approach is usually the only way to describe a rough surface. In line with the continuous approach, Flack & Schultz (2010) analysed data from several surface roughnesses and reported that the equivalent sand roughness is given by $k_s = 4.43 k_{rms}(1 + sk)^{1.37}$, where k_{rms} and sk are the root mean square and the skewness of the surface heights, respectively. Nikora *et al.* (1998) reported that the heights of the surface roughness of a gravel bed are nearly Gaussian with an isotropic second-order structure function $D(\ell)$ proportional to ℓ^{2H} for sufficiently small spatial separation ℓ, where H is the Hurst exponent, which those authors determined to be 0.79 for a water-worked gravel bed. This behaviour indicates that, at sufficiently small spatial scales, the surface roughness has the properties of a self-affine fractal surface (Turcotte 1997; Meakin 1998). Other examples of surface roughness showing self-affinity are the surface of the planet Mars (Orosei *et al.* 2003) and fracture surfaces (Ponson *et al.* 2006).

The effect of roughness on the flow can be assessed by the downward shift ΔU^+ it produces in the logarithmic velocity profile with respect to the logarithmic law of turbulent flow on a smooth wall, known as the roughness function, which is related to the friction factor. Hereinafter, the superscript + denotes a quantity which is made dimensionless by the friction velocity u_τ or by the viscous length ν/u_τ, where ν is the kinematic viscosity. Over the past few decades, several studies have investigated the effect of roughness on ΔU^+. Napoli, Armenio & De Marchis (2008) considered irregular two-dimensional roughness and showed that ΔU^+ scales with the effective slope ES given by the spatial

https://doi.org/10.1017/jfm.2025.61 Published online by Cambridge University Press

average of the absolute value of the streamwise surface slope. It can be shown that ES is twice the solidity Λ (Schlichting 1936) defined as the ratio between the sum of the area of all roughness elements projected in the plane perpendicular to the flow direction and the horizontal area. Leonardi *et al.* (2003) used direct numerical simulation (DNS) to study turbulent flow on two-dimensional square bars placed orthogonally to the flow and found results from which it can be deduced that the maximum of ΔU^+ is obtained for $\Lambda = 0.125$. According to MacDonald *et al.* (2016), the value $\Lambda = 0.15$ separates the sparse regime, where ΔU^+ increases with Λ, from the dense regime, where ΔU^+ decreases with Λ. This value of Λ is not very different from 0.125, which maximises ΔU^+ according to the results of Leonardi *et al.* (2003). In a numerical study of flow in pipes characterised by a three-dimensional sinusoidal corrugation, Chan *et al.* (2015) found that ΔU^+ depends on a combination of both the roughness height and the effective slope.

Forooghi *et al.* (2017) numerically studied the flow over a rough surface created by distributing roughness elements over a flat surface and found that the flow resistance depends on several parameters, including the skewness and the distribution of the roughness elements, with the staggered distribution giving results closer to a random distribution. The importance of the skewness of the roughness height has also been pointed out by Busse, Thakkar & Sandham (2017) who studied the hydrodynamic properties of a graphite surface and a grit-blasted surface and found that positive skewness provides the greatest resistance to flow. Barros, Schultz & Flack (2018) tested surfaces characterised by power spectral slope proportional to k^p finding that the surface with the lowest slope ($p = -0.5$) has the largest drag, although this case has the smallest k_{rms}. This was attributed to the presence of low-wavelength features contributing to k_{rms} but not to the drag. Forooghi *et al.* (2018) improved the parametric forcing model of Busse & Sandham (2012) to be able to reproduce the effect of several rough surface characteristics, including skewness. Stewart *et al.* (2019) studied experimentally the hydrodynamic properties of a self-affine surface roughness characterised by three different PSDs with scaling exponents -1, $-5/3$ and -3. They reported that the friction factor increases as the scaling exponent increases. Guo-Zhen *et al.* (2020) studied the flow on a regular three-dimensional sinusoidal wall and showed that ΔU^+ scales with the product between the amplitude of the roughness and ES. The case of irregular three-dimensional roughness was also considered by Ma, Alamé & Mahesh (2021), who carried out DNS on the surface corresponding to the experiments of Flack, Schultz & Barros (2020).

The importance of roughness distribution, in addition to roughness height, as a factor affecting the roughness function has been highlighted by Thakkar, Busse & Sandham (2017) in their DNS studies of flow on surface roughness. A method for determining which roughness parameter has the greater influence on the roughness function was also presented. Excellent agreement with the results of Nikuradse (1933) was obtained by Thakkar, Busse & Sandham (2018) in a study of turbulent flow over an industrial grit-blasted surface. Busse & Jelly (2020) studied the effect of surface anisotropy, defined as the ratio between the streamwise and spanwise correlation lengths, and found that as this ratio decreases, ΔU^+ increases. De Marchis *et al.* (2020) considered three-dimensional rough surfaces created by superimposing random amplitude sinusoids and determined the flow characteristics using large-eddy simulation. The study showed that no single parameter of the roughness geometry is sufficient to describe the roughness function, but the results showed that ΔU^+ can be adequately described by a suitable combination of ES and k^+_{rms}. Portela, Busse & Sandham (2021) used Fourier filtering to create different rough surfaces from a baseline surface. They found that existing correlations mostly predict the roughness function, but also emphasised that these correlations should include information about the spectral distribution to improve accuracy. Recently, the influence of the effective spanwise

https://doi.org/10.1017/jfm.2025.61 Published online by Cambridge University Press

slope on ΔU^+ was analysed by Jelly *et al.* (2022), who reported that ΔU^+ decreases with the effective spanwise slope when all other geometric parameters are held constant. This is probably related to the increasing two-dimensionality of the roughness as the spanwise slope decreases, which creates more obstacles to the flow.

Yang *et al.* (2022) studied the flow in a minimal channel and reported that, for an irregular roughness, sufficiently accurate predictions can be obtained if the channel size is large enough to contain more than 90 % of the original roughness height spectral energy. Recently, methods based on artificial neural networks are increasingly being used to predict relevant hydrodynamic features of surface roughness, as in Yang *et al.* (2023*a*), who constructed a model to predict equivalent sand roughness based on the probability density function and power spectrum of the rough surface. Yang *et al.* (2023*b*) analysed different rough-wall models and concluded that empirical correlations are effective when calibrated and applied to the same type of roughness. Machine learning and physics-based models were also analysed: the former improve as the amount of data increases; the latter are more adaptable, but require all physical aspects to be identified. In a recent study, Busse & Jelly (2023) analysed rough surfaces with very high skewness and observed a saturation of roughness effects at the limits of very high skewness. Ramani *et al.* (2024) critically examined the dependence of the friction factor on the effective slope and showed from experimental measurements that scale roughness less than three times the viscous length has a weak effect on drag, despite its large contribution to ES. The larger contribution to drag comes from the slope due to large scale features.

Previous studies have shed much light on flows on rough surfaces, but the results are still inconclusive, so there is still room for further knowledge in this area. In this context, the present work aims to better understand how three-dimensional irregular roughness affects the roughness function. The analysis is carried out by DNS and focuses on the effect of the PSD and the root mean square of the surface roughness heights on the flow. In § 2 the geometry of the surface roughness is defined and the numerical approach is described. In § 3 the results of the study are illustrated and in § 4 some conclusions are drawn.

2. The rough surface and the numerical approach

The turbulent flow in a channel with a rough bottom wall is analysed in this study. All lengths that appear from here on have been made dimensionless using the depth h of the channel, except where a plus symbol appears in superscript for variables expressed in wall units. A Cartesian coordinate system (x, y, z) is introduced as a reference, with the x–z plane located at the mid-level of the rough bottom wall and the x axis pointing in the direction of the flow. The sizes of the fluid domain are denoted as L_x, $L_y = 1$ and L_z in the x, y and z directions, respectively. The bottom wall is characterised by periodic displacements with respect to $y = 0$ with periods equal to L_x and L_z along the x and z directions, respectively. Therefore, the surface heights η can be expressed in Fourier series:

$$\eta(x, z) = \sum_{m=-M}^{M} \sum_{n=-N}^{N} f(m, n) \exp[\mathrm{i}(m\kappa_x x + n\kappa_z z)], \tag{2.1}$$

where m and n are integers, i is the imaginary unit, $f(m, n)$ is a complex number, $\kappa_x = 2\pi/L_x$ and $\kappa_z = 2\pi/L_z$. Assuming that the spatial average of η in the x and z directions is zero, it follows that $f(0, n) = f(m, 0) = 0$ regardless of the values of m and n. The spatial autocorrelation function of the surface roughness $R(\ell_x, \ell_z)$, where ℓ_x and ℓ_z are

https://doi.org/10.1017/jfm.2025.61 Published online by Cambridge University Press

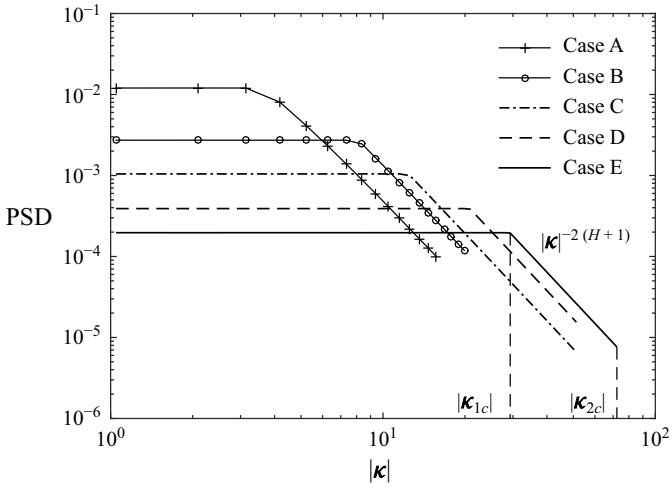

Figure 1. Power spectral density of rough surfaces versus wavenumber magnitude ($H = 0.8$) for $k_{rms} = 1$.

the spatial separations along the x and z directions, respectively, is given by

$$R(\ell_x, \ell_z) = \frac{1}{L_x L_z} \int_0^{L_x} \int_0^{L_z} y(x, z) y(x + \ell_x, z + \ell_z) \, \mathrm{d}x \, \mathrm{d}z$$
$$= \sum_{m=-M}^{M} \sum_{n=-N}^{N} |f(m, n)|^2 \exp[\mathrm{i}(m k_x \ell_x + n k_z \ell_z)]. \tag{2.2}$$

Using equation (2.2), the root mean square of the surface height η is given by $k_{rms} = \sqrt{R(0, 0)}$. The PSD, given by the Fourier transform of the spatial autocorrelation function, can be written as follows:

$$\mathrm{PSD}(m\kappa_x, n\kappa_z) = \frac{1}{4\pi^2} L_x L_z |f(m, n)|^2. \tag{2.3}$$

It is assumed that the PSD depends on the magnitude of the wavenumber $|\boldsymbol{\kappa}| = \sqrt{(m^2\kappa_x^2 + n^2\kappa_y^2)}$. This choice is made because several natural and artificial roughnesses have a PSD that follows the power law $|\boldsymbol{\kappa}|^{(-2H-d)}$ over a range of wavenumbers, typical of a self-affine surface characterised by the Hurst exponent H ($0 < H \leq 1$), where d is the Euclidean dimension, which in this case is equal to 2 (Meakin 1998). Note that since the PSD depends only on the magnitude of the wavenumber, all surface roughness quantities, including the effective slope, are independent of spatial direction. Five different PSDs were used to generate the surface roughness, the shape of which is shown in figure 1 for $k_{rms} = 1$.

It is observed that at low wavenumbers the PSD is constant, as observed for different types of roughness (Stewart *et al.* 2019). It then follows a power-law decay that ends with an abrupt cut-off. The power density spectra are distinguished by the wavenumbers $\boldsymbol{k}_{1c}$ and $\boldsymbol{\kappa}_{2c}$ whose modules are shown in table 1 along with the corresponding wavelengths λ_{1c} and λ_{2c}, while the Hurst exponent H has been set to 0.8, which is close to the 0.79 reported by Nikora *et al.* (1998) for natural water-worked beds.

For each spectrum, several surfaces have been generated by varying k_{rms}, assuming that the surface heights η follow a Gaussian distribution so that the skewness of the rough

https://doi.org/10.1017/jfm.2025.61 Published online by Cambridge University Press

Case	$\lvert\boldsymbol{k}_{1c}\rvert$	$\lvert\boldsymbol{k}_{2c}\rvert$	λ_{1c}	λ_{1c}^{+}	λ_{2c}	λ_{2c}^{+}
A	4.18	16.75	1.50	751	0.375	187
B	8.37	20.94	0.75	375	0.30	150
C	12.56	52.36	0.50	250	0.12	60
D	20.94	52.36	0.30	150	0.12	60
E	29.32	73.30	0.21	107	0.09	43

Table 1. Characteristic wavenumbers and wavelengths of the PSD of the rough surfaces.

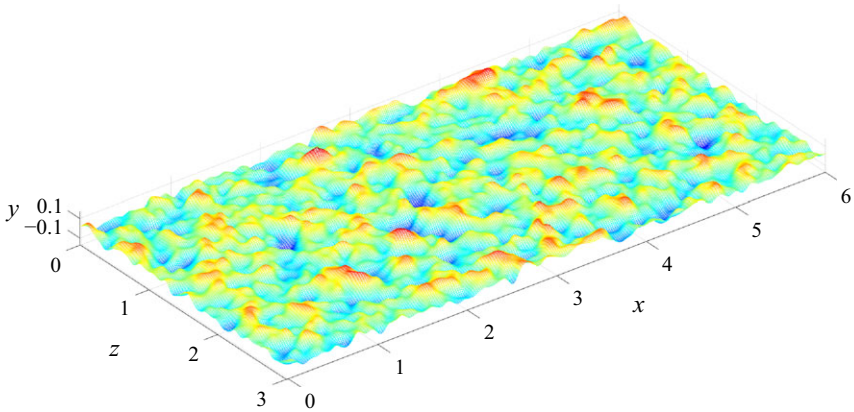

Figure 2. Example of a rough surface belonging to case C for $k_{rms} = 0.04$.

surface approximately vanishes. As an example, figure 2 shows the surface roughness for the case C (see table 1) with $k_{rms} = 0.04$.

The study was carried out by numerically solving the continuity and momentum equations. Using the friction velocity u_τ as the velocity scale and ϱu_τ^2 as the pressure scale, where ϱ is the fluid density, these equations take the following dimensionless form:

$$\frac{\partial u_j}{\partial x_j} = 0, \tag{2.4}$$

$$\frac{\partial u_i}{\partial t} + \frac{\partial u_i u_j}{\partial x_j} = -\frac{\partial p}{\partial x_i} + \frac{1}{R_\tau}\frac{\partial^2 u_i}{\partial x_j \partial x_j} + \delta_{1,i}, \tag{2.5}$$

where $u_i\,(i = 1, 2, 3)$ are the velocity components (also referred to as u, v, w respectively), p is the pressure, $R_\tau = u_\tau h/\nu$ is the Reynolds number, the subscripts $j = 1, 2$ and 3 denote the directions x, y and z, respectively, $\delta_{1,i}$ is the Kronecker δ, and repeated subscripts are used to denote a summation. The numerical approach is based on centred second-order finite differences on a Cartesian staggered grid. The time advancement is based on a third-order Runge–Kutta method for the convective terms and on the Crank–Nicolson scheme for the viscous terms. Periodic boundary conditions are applied along the x and z directions. On the bottom wall, the no-slip condition $(u, v, w) = (0, 0, 0)$ is enforced, while on the top wall the free shear stress condition $(\partial u/\partial y, v, \partial w/\partial y) = (0, 0, 0)$ is enforced as in Yuan & Piomelli (2014*b*). The boundary condition on the bottom rough surface is imposed by an immersed boundary method similar to that used by Leonardi *et al.* (2003).

https://doi.org/10.1017/jfm.2025.61 Published online by Cambridge University Press

In all simulations, the dimensionless lengths of the fluid domain L_x and L_z are set to 6 and 3, respectively, and the Reynolds number R_τ is set to 500. The size of the numerical grid (n_x, n_y, n_z) varied from (300, 220, 300) to (480, 400, 360) as shown more in detail in tables 2–6 in Appendix A. The grid spacing in the x direction is smaller than or equal to 10 wall units. Spatial resolution of about 10 wall units in the x direction has been used by Guo-Zhen *et al.* (2020) who used a spacing of 11 wall units in the x direction. A spacing of 8–10 wall units in the flow direction has been used with the present code to study oscillatory flow on an irregular rough bed in Dunbar *et al.* (2023). In that study, the DNS results were compared with experimental measurements using a laser Doppler anemometer in a large oscillating flow tunnel, with good agreement even for the higher-order statistics of the velocity fluctuations. The spatial resolution in the flow direction is 6 wall units with 480 meshes in the x direction for the simulations of case E, which has the highest wavenumbers, corresponding to 7 grid points at the shortest wavelength. Regarding the grid convergence, for example, in case E, for $k_{rms} = 0.075$, increasing the number of grid points in the x direction from 360 to 480, the variation of ΔU^+ was less than 0.1 over a ΔU^+ of about 10.8, which is less than 1 %.

The grid spacing in the y direction is not constant, as a number of grid points are clustered near the rough surface, where large gradients exist. More specifically, in the layer between the lowest trough and the highest peak of the roughness, the grid spacing Δy^+ was kept below 1.

3. Discussion of the results

The roughness function was determined by fitting the logarithmic law of the wall, expressed by the (3.1), to the spatial and temporal average of the streamwise velocity data:

$$u^+ = \frac{1}{k}\log(y^+ - d^+) + C - \Delta U^+. \tag{3.1}$$

In (3.1), $k = 0.4$ is the von Kármán constant, $C = 5$ is a constant and d^+ is a shift away from the plane $y^+ = 0$ to maximise the quality of the logarithmic fit. The values of d^+ and ΔU^+ were estimated by the least squares method in the interval $40 \leqslant (y^+ - d^+) \leqslant 150$. To check the sensitivity of ΔU^+ to the interval used, increasing the lower bound to 50 resulted in a difference of less than 0.1. A similar range was considered by Forooghi *et al.* (2017) who used $y^+ = 30$ as the lower bound and $y/h = 0.3$ as the upper bound. In Appendix A, tables 2–6 show the parameters of the rough surfaces and the numerical values of ΔU^+.

Figure 3(*a*) shows some semi-logarithmic plots of the velocity profiles for case E, from which it is evident that the velocity decreases as k_{rms} increases.

As shown in tables 2–6, some of the rough surfaces are characterised by a relatively large $S_{y5\times5}$ (Thakkar *et al.* 2017), which may hinder the similarity of velocity profiles normally observed outside the region directly affected by the roughness. Figure 3(*b*) shows the velocity defect profiles for case E, which is that characterised by the largest roughness heights. It can be seen that the velocity defect profiles approximately follow the trend of the smooth-wall case with some larger deviations for $k_{rms} = 0.085$. To explain why, despite the large $S_{y5\times5}$, there is still a similarity between the velocity profiles of the smooth- and rough-wall cases, a new measure of roughness height, called $H_{5\,\%5\times5}$, is introduced. This height is based on the difference between the position y_u, above which the roughness covers less than 5 % of the total surface x–z, and y_l, below which the fluid covers less than 5 % of the total surface. Height $H_{5\,\%5\times5}$ is determined as $S_{y5\times5}$, i.e. the surface is divided into 5×5 tiles and for each of these y_u and y_l are determined. Finally, $H_{5\,\%5\times5}$ is calculated as the arithmetic mean of $y_u - y_l$ of all the tiles. It can be observed that $S_{y5\times5}$ is

https://doi.org/10.1017/jfm.2025.61 Published online by Cambridge University Press

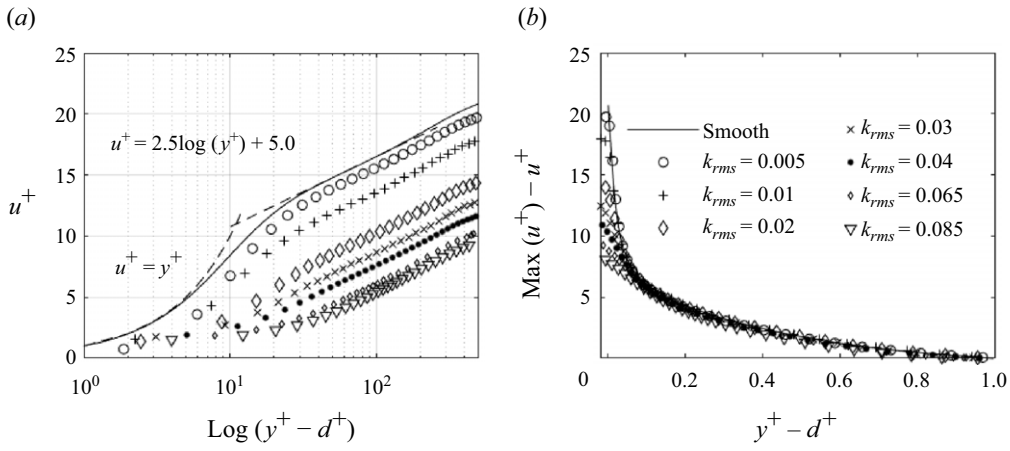

Figure 3. (*a*) Semi-logarithmic plot of the velocity profiles for case E. (*b*) Velocity defect profiles for case E.

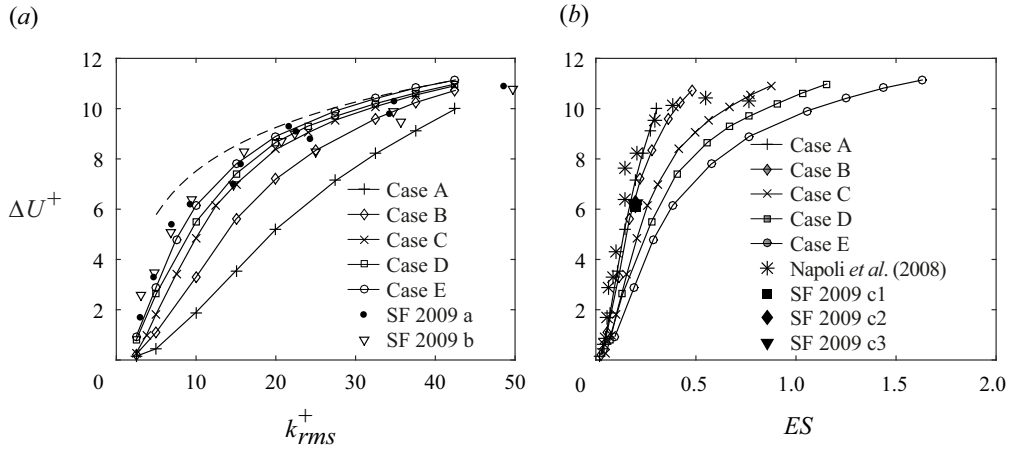

Figure 4. (*a*) Roughness function versus k^+_{rms}. Here SF 2009a and SF 2009b refer to the data of Schultz & Flack (2009) for $\alpha = 45°$ and $\alpha = 22°$, respectively. The dashed curve is described by the equation $(1/k)\log(k^+_{rms}) + 1.76$. (*b*) roughness function versus ES. Here SF 2009c1,c2,c3 refer to the highest-Reynolds-number cases of Schultz & Flack (2009) for $\alpha = 11°$.

obtained as the special case when the percentage is set to zero. The reason for introducing this measure of roughness height is that for the roughness to break the similarity of the velocity profiles, it is not enough for its height to be large; the roughness must also cover a sufficiently large proportion of the total area. The value of 5 % of the total area is chosen as the value below which it seems reasonable that the roughness will not have a significant effect on the velocity defect profiles. In tables 2–6 it can be seen that $H_{5\,\%5\times5}$ is about half of $S_{y5\times5}$, which can explain why the similarity of the velocity profiles is maintained. As a further check on the effect of roughness height, the mean velocity profiles were also computed using the intrinsic spatial average (average over the fluid domain only) and for case E_{10} the difference in ΔU^+ with respect to the spatial average was only about 0.3 %.

In figure 4(*a*), where ΔU^+ is plotted against k_{rms} for cases A–E, it can be seen that ΔU^+ scales with k_{rms} only within each case, highlighting that the roughness function is influenced by additional surface properties depending on the PSD. As we move from

https://doi.org/10.1017/jfm.2025.61 Published online by Cambridge University Press

case A to case E, for a fixed k_{rms}, ΔU^+ increases first rapidly and then slowly, so there is not much difference between cases D and E, which are characterised by the largest wavenumbers. For comparison, figure 4(*a*) also shows data from Schultz & Flack (2009), who performed experiments with a rough wall made of square-based pyramids, considering three different cases of the angle of inclination α of the pyramid diagonal: 45°, 22° and 11°. Figure 4(*a*) shows only the data for α equal to 45° and 22° as a function of k^+_{rms}, determined as $k^+_{rms} = k^+_t/\sqrt{18}$, where k^+_t is the height of the pyramid. When comparing the two datasets, it should be noted that in the present study ES changes as k^+_{rms} increases, whereas in Schultz & Flack (2009) ES is held constant and is equal to 1 for $\alpha = 45°$ and 0.40 for $\alpha = 22°$. We note that despite the large difference in α between SF 2009a and SF 2009b, these experimental data show no clear difference between them. On the other hand, the present results show a gap in ΔU^+ between the different power spectra, albeit small in some cases. Nevertheless, the present results show a trend that is in line with that of Schultz & Flack (2009), especially for cases D and E, and the relatively small differences can be explained by the different values of ES, as described below. For case E, in the interval $k^+_{rms} = 2.5-10$, the effective slope ranges from 0 to 0.4, i.e. it is smaller than that of Schultz & Flack (2009) (0.4–1), so that the present ΔU^+ is generally smaller than that of the aforementioned study. In the range $k^+_{rms} = 10-25$, the present values of ES vary approximately between 0.4 and 1, then the effective slopes are similar and we find that the two ΔU^+ are also similar. Finally, for $k^+_{rms} > 25$ the present effective slope is larger than that of Schultz & Flack (2009), and hence the present ΔU^+ are larger than those of the aforementioned study. This comparison shows that the present results are generally consistent with those of Schultz & Flack (2009), even from a quantitative point of view.

As shown in figure 4(*b*), even when ΔU^+ is plotted against the effective slope ES, the data collapse on the same curve only within each case. This result contrasts with that of Napoli *et al.* (2008), also shown in figure 4(*b*), who obtained data collapse on the same curve regardless of the roughness amplitude.

Figure 4(*a*) shows that cases A and B are quite far apart, whereas in figure 4(*b*) they are very close to each other and together they are also close to most of the data from Napoli *et al.* (2008). Therefore, based on cases A and B, one could conclude that ΔU^+ scales with ES. This shows that a possible explanation for ΔU^+ scaling with ES in Napoli *et al.* (2008) could be the use of surface roughness with a power density spectrum characterised by small wavenumbers, as in cases A and B. If only surface roughness with power density spectra characterised by very high wavenumbers is considered, as in cases D and E, different conclusions can be drawn. In fact, as figure 4(*a*) shows, the data from cases D and E appear very close to each other when plotted against k^+_{rms}, so one could claim that in general ΔU^+ scales with k^+_{rms}, which is clearly not true when looking at the overall picture of the results.

Since the data from Schultz & Flack (2009) shown in figure 4(*a*) scale with k^+_{rms}, it is expected the rough surface is also characterised by large wavenumbers. Taking the wavenumber relative to the diagonal of the pyramid used as the roughness element as the reference wavenumber and scaling it by the thickness of the boundary layer, the wavenumbers range from 64 to 294 for $\alpha = 45°$ and $\alpha = 22°$ and from 31 to 53 for $\alpha = 11°$. Again, this result shows that scaling with roughness height is associated with high wavenumbers. Indeed, the case with $\alpha = 11°$ did not scale with either k_{rms} or ES. The term 'waviness' regime was introduced by the authors for this case to indicate flows on surfaces with long wavelengths where ΔU^+ does not scale with roughness height. However, the effect of the wavenumber is also clearly visible within the data with $\alpha = 11°$. In fact, the case $\alpha = 11°$ consists of three subsets of data, each characterised by an approximately

https://doi.org/10.1017/jfm.2025.61 Published online by Cambridge University Press

constant wavenumber, and it can be seen that within each of these subsets, ΔU^+ scales with k^+_{rms}. Among these three cases, that characterised by the largest wavenumber has the largest ΔU^+ for a given roughness size (see figure 11 of Schultz & Flack (2009)). The values of ΔU^+ obtained for the largest Reynolds numbers from these three subsets are shown in figure 4(*b*) and it can be seen that they are close to the present results obtained for the surface characterised by low wavenumbers.

In general, the rate of increase of ΔU^+ with k^+_{rms} tends to decrease as this quantity increases (note that ES also increases with k^+_{rms}). This is because the increase in k^+_{rms} causes an increase in $S_{y5\times5}$ resulting in deep depressions where the flow has recirculation zones enclosed between ridges with little interaction with the external flow. In these cases, only the upper part of the roughness makes a significant contribution to drag, and a further increase in k_{rms} will not result in a significant increase in ΔU^+. This behaviour is related to the asymptotic tendency of ΔU^+ towards the logarithm of k^+_{rms}, typical of flows approaching the fully rough regime. In the case of the Nikuradse sand roughness, reaching the fully rough regime is indicated by the roughness function varying according to the equation

$$\Delta U^+ = \frac{1}{k}\log\left(k_s^+\right) + a, \tag{3.2}$$

with $a = -3.5$. If k_{rms} is used instead of k_s, the roughness function in the fully rough regime still obeys an equation similar to (3.2) where k_s^+ is replaced by k^+_{rms} and a takes a different value from that given above.

In figure 4(*a*) it can be seen that as k^+_{rms} increases, the curves tend to converge, and it appears that overall they tend to converge towards the curve of (3.2) with $a = 1.76$ and k_s^+ replaced by k^+_{rms} (see the dashed line in figure 4(*a*)). Since for a fixed value of k^+_{rms} each curve is characterised by a different value of ES, and yet the curves become closer and closer together, it follows that ES does not affect the behaviour of the curves for large k^+_{rms}. This is because as k^+_{rms} increases, so does ES, and at some point ΔU^+ saturates with respect to ES, after which ΔU^+ starts to scale only with k^+_{rms}. This is consistent with the statement of Schultz & Flack (2009) that if the roughness slope is steep enough, the roughness function will scale completely to the roughness height.

To provide a further proof of the independence of ΔU^+ on ES, we focus on case E to prove by a test that ΔU^+ scales with k^+_{rms} for large values of this variable. To perform this test, the rough surface of case E_8 ($k_{rms} = 0.065$) was used to perform an additional simulation with $R_\tau = 654$ which gives $k^+_{rms} = 42.5$. This new simulation has the same k^+_{rms} as that of case E_{10} at $R_\tau = 500$ ($k_{rms} = 0.085$, $k^+_{rms} = 42.5$) but ES of case E_8. By comparing the result of this simulation with that of case E_{10} it can be verified if ΔU^+ scales only with k^+_{rms} or if there is also an influence of ES. The result of this additional simulation shows that for $k_{rms} = 0.065$ and $R_\tau = 654$ the roughness function takes a value of 11.16, while for $k_{rms} = 0.085$ and $R_\tau = 500$ a value of 11.14 was obtained. The difference in ΔU^+ is about 0.2 % and is very small considering that it results from a difference in ES of 30 %. This shows that ΔU^+ scales with k^+_{rms}. This result is only valid for case E; for the other cases shown in table 1, a test like the previous one would have shown a dependence of ΔU^+ on ES especially for cases A and B.

Many studies have shown that for a fixed value of roughness height, ΔU^+ increases for ES less than a certain value, reaches a maximum and then decreases as ES is further increased. This decrease in ΔU^+ occurs because for large ES the roughness enters the dense regime, where the roughness elements shelter each other from the flow. This may lead to the conclusion that the previously shown independence of ΔU^+ from ES in

https://doi.org/10.1017/jfm.2025.61 Published online by Cambridge University Press

the interval $k_{rms} = 0.065-0.085$ is merely a consequence of ΔU^+ being close to its maximum, so that if k_{rms} is increased further, the dependence on ES could emerge and cause the deviation of ΔU^+ from the fully rough asymptote. In this regard, note that as k_{rms} increases, the wavenumbers of the rough surface remain unchanged, as the shape of the power density spectrum is constant for each of the cases shown in table 1. Therefore, the roughness does not become more densely packed and no decrease in ΔU^+ with ES is observed. An example where an increase in ES led to a decrease in ΔU^+ can be found in MacDonald *et al.* (2016), where the roughness height was kept constant and the increase in ES was obtained by decreasing the roughness wavelength. Those authors showed that ΔU^+ peaks at about $ES = 2\Lambda \approx 0.3$ (see also figure 5*a* in Chung *et al.* (2021)) and then decreases with ES. Further support for the hypothesis of independence of ΔU^+ from ES comes from previous studies which, in the case of irregular rough surfaces, have shown a monotonic increase of ΔU^+ with ES for a fixed roughness height, with a tendency to reach a plateau at large ES (Yuan & Piomelli 2014*a*; Kuwata & Nagura 2020). This behaviour is also observed in the present case, as can be seen in the figure 6, which is discussed in the following. This result, combined with the constancy of the shape of the PSD, gives confidence that as k_{rms} increases, ΔU^+ is unaffected by ES for large effective slopes. Despite the above evidence for the independence of ΔU^+ from ES, it is possible to further verify it for k_{rms} larger than considered here by performing simulations for higher k_{rms} and larger Reynolds numbers. However, this is left to future studies on this topic.

Having shown that for large values of ES the roughness function scales with k^+_{rms}, it is possible to determine the equivalent sand roughness which, based on the previous discussion, is appropriate for large effective slopes such that ΔU^+ saturates when expressed as a function of ES. The equivalent Nikuradse sand roughness can be calculated as $k^+_s = \xi k^+_{rms}$, where $\xi = \exp[k(a + 3.5)]$ and a is the constant in equation (3.2) with k^+_s replaced by k^+_{rms} as the independent variable. In figure 4*(a)*, the constant a of case E is about 1.76, so using the previous equation we get $\xi \approx 8.2$. This value is very different from the $\xi = 4.43$ reported by Flack & Schultz (2010). Schultz & Flack (2009), using their experimental data shown in the present figure 4*(a)*, obtained k_s equal to 1.5 times the height of the pyramid. This relationship, expressed in terms of k_{rms}, becomes $k^+_s = 6.36k^+_{rms}$ which is still somewhat far from the current result. However, it should be noted that other studies have also found ξ to be approximately equal to 8. Based on a study of turbulent flow on a regular three-dimensional rough surface described by the product of two cosine waves of the type $\eta = A\cos(2\pi x/L_w)\cos(2\pi z/L_w)$ with wavelength L_w, Guo-Zhen *et al.* (2020) reported that in the fully rough regime $k^+_s = 3.7A^+$. Since k_{rms} of this surface is equal to $0.5A$, we can write $k^+_s = 7.4k^+_{rms}$, which is not too far from the present result. Chan *et al.* (2015) carried out a study of flow in a pipe made rough by sinusoidal undulations such as those described above and reported $k^+_s = 4.1A^+$. This equation, when written in terms of k^+_{rms}, reads as $k^+_s = 8.2k^+_{rms}$, therefore consistent with the present result. The finding that for substantially different roughnesses, regular or irregular, the relationship between k_{rms} and k_s in the fully rough regime is expressed by a very similar relationship suggests that k_{rms} is an appropriate and fairly general measure of surface roughness.

An equation for the roughness function can also be provided for the transitional rough regime, but parameters in addition to k_{rms} are required. The surface roughness considered in this study is characterised by three parameters, k_{rms}, $|\boldsymbol{\kappa}_{1c}|$ and $|\boldsymbol{\kappa}_{2c}|$, but as shown below, a good description of ΔU^+ can be obtained with only two parameters by replacing $|\boldsymbol{\kappa}_{1c}|$ and $|\boldsymbol{\kappa}_{2c}|$ with ES. In fact, over a wide range of k_{rms} and ES, the roughness function can

https://doi.org/10.1017/jfm.2025.61 Published online by Cambridge University Press

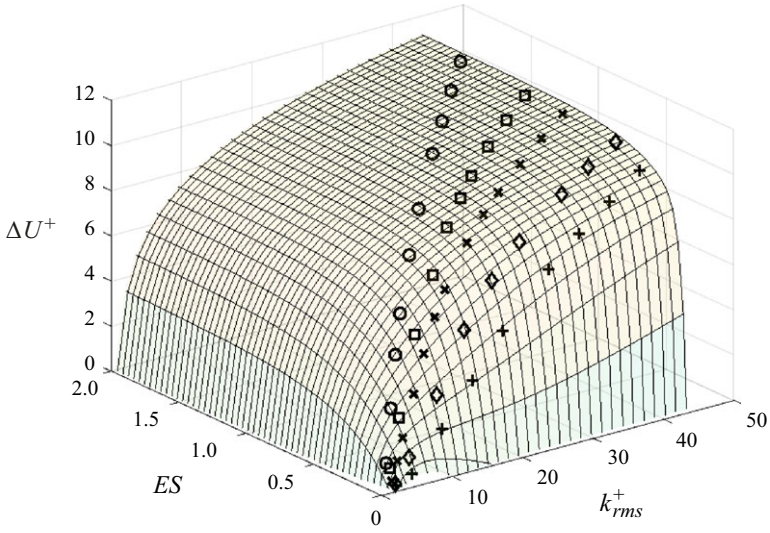

Figure 5. Numerical values of ΔU^+ versus (k^+_{rms}, ES) and comparison with (3.3). For the legend, refer to figure 4.

be approximately described by the equation

$$\Delta U^+ = \frac{1}{k}\log(k^+_{rms}) + 1.76 - 3.21\exp(-3.51ES) \\ -0.42k^+_{rms}\exp[-0.54k^+_{rms}ES]. \tag{3.3}$$

Equation (3.3) has four terms. The first term plus the second gives ΔU^+ in the fully rough regime when ES is large enough to cause the saturation of the roughness function. The third term provides a correction to the previous asymptote when ES does not take large values. Finally, the fourth term is introduced to reproduce the roughness function in the transitional rough regime. This term is therefore a measure of the deviation of the flow conditions from the fully rough regime. It should be noted that the region of very small ES and large k^+_{rms} was not explored in this study, so equation (3.3) is not reliable for these types of rough walls. The goodness of the fit of this equation to the numerical data can be seen in figure 5 and is evidenced by a coefficient of determination $R^2 = 0.99$. Given the good quality of the fit of (3.3) to the present data, it is worth presenting some plots of ΔU^+ as a function of k^+_{rms} where ES is constant, and of ΔU^+ as a function of ES where k^+_{rms} is constant, shown in figure 6. To be more reliable, these graphs have been drawn through the areas covered by numerical data. In figure 6(*a*) we observe that the larger ES the closer the curve is to the fully rough asymptote of case E and the earlier the fully rough regime is reached by increasing k^+_{rms}. In figure 6(*b*) we see that for a fixed value of k^+_{rms}, as the effective slope increases, ΔU^+ also increases, but it reaches a plateau at about $ES = 0.75$, a result that can also be seen in figure 5.

This picture differs from many studies which report that for a fixed roughness height ΔU^+ reaches a maximum at $ES \approx 0.3$ and then decreases with ES. However, the present results are consistent with those of other studies (Yuan & Piomelli 2014*a*; Kuwata & Nagura 2020) on flows over an irregular rough surface. Therefore, this behaviour can be considered as a characteristic specific to irregular rough surfaces. A critical value of ES for irregular rough surfaces, above which ΔU^+ decreases with ES, has not been identified. One of the difficulties in identifying it lies in the considerable computational

https://doi.org/10.1017/jfm.2025.61 Published online by Cambridge University Press

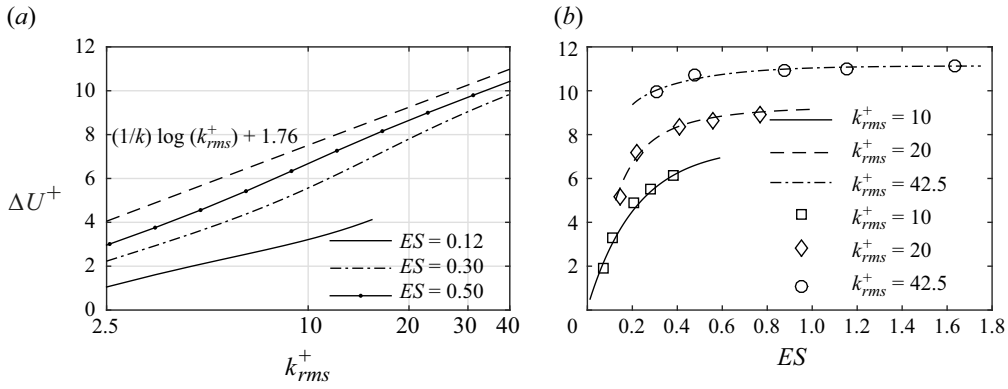

Figure 6. (*a*) Examples of the trend of ΔU^+ with respect to k^+_{rms} for ES fixed. (*b*) Examples of the trend of ΔU^+ with respect to ES for k^+_{rms} fixed. The markers show the numerical data, and the lines are described by (3.3).

effort involved in solving the governing equations on a rough surface characterised by increasingly large wavenumbers.

Empirical equations describing ΔU^+ have also been proposed by Chan *et al.* (2015), De Marchis *et al.* (2020) and Guo-Zhen *et al.* (2020), among others. These equations can be written in the following general form:

$$\Delta U^+ = \alpha\ \log(k^+_{rms}) + \beta\ \log(ES) + \gamma. \tag{3.4}$$

In De Marchis *et al.* (2020) $\alpha = \beta = 1/k$, while in Guo-Zhen *et al.* (2020) $\alpha = \beta = 2.66$. In the latter case, the condition that in the fully rough regime ΔU^+ varies as $(1/k)\log(k^+_{rms}) + \text{const.}$ is not perfectly satisfied. Fitting equation (3.4) to the present data with $\alpha = \beta = 1/k$ gave an R^2 of 0.87, which is significantly lower than that obtained with equation (3.3). In this case, the relatively poor quality of the fit is mainly due to the presence of only γ as a fitting coefficient. Chan *et al.* (2015) imposed only $\alpha = 1/k$ in (3.4), and fitting the equation to their data gave $\beta = 1.12$ and $\gamma = 0.96$. Note that Chan *et al.* (2015) used the spatial average of the absolute value of the surface heights as a measure of the magnitude of the surface roughness, so the coefficient γ has been corrected to account for the fact that equation (3.4) is written in terms of k^+_{rms}. Using the coefficients $\alpha = 1/k$, $\beta = 1.1$ and $\gamma = 0.96$, which are very close to those of Chan *et al.* (2015), the goodness of fit of equation (3.4) to the present data is measured by an R^2 equal to 0.95. This indirectly shows that the present data are consistent with those of Chan *et al.* (2015), since they are described by two similar empirical equations. It should be noted, however, that (3.4) is formally valid only in the fully rough regime; indeed for a fixed value of ES, ΔU^+ varies as $(1/k)\log(k^+_{rms}) + \text{const.}$ On the other hand, (3.3) contains a term capable of describing ΔU^+ in the transitional rough regime, where the roughness function does not follow the logarithmic law.

4. Conclusions

In this study, numerical simulations of turbulent flow were used to analyse the effect of irregular surface roughness on the roughness function. Several Gaussian rough surfaces were generated using five different forms of the PSD and varying the root mean square of the surface heights (k_{rms}) for each.

The results show that in general neither k_{rms} nor ES, considered singularly, are sufficient to describe the roughness function. However, for PSD with low wavenumbers,

https://doi.org/10.1017/jfm.2025.61 Published online by Cambridge University Press

ΔU^+ tends to scale with ES, while as wavenumbers increase, ΔU^+ tends to scale with k^+_{rms}, and this occurs even for small values of ES, for which it is commonly reported in the literature not to scale with roughness height. This result is consistent with that of Schultz & Flack (2009), who found that for short-wavelength three-dimensional roughness, the roughness function scales almost entirely with the roughness height, whereas for long wavelengths no clear behaviour was found, as the trend of ΔU^+ depends on the specific value of the wavenumber.

In general, for a fixed value of k^+_{rms}, ΔU^+ increases as the PSD expands to large wavenumbers but at a rate that decreases as the magnitude of the wavenumbers increases. Consistent with the above result, the trend of ΔU^+, plotted as a function of ES for a constant k^+_{rms}, shows a monotonic increase with a tendency to asymptote at a constant value. This behaviour differs from that reported in numerous previous studies, which indicated that ΔU^+ is maximised for certain values of ES. In the light of other studies (Yuan & Piomelli 2014*a*; Kuwata & Nagura 2020), which gave results comparable to the present ones, it seems reasonable to conclude that this discrepancy is due to the irregularity of the roughness.

For a fixed shape of the PSD, as k^+_{rms} increases, the curves describing ΔU^+ saturate with respect to ES and eventually tend to asymptote the equation $\Delta U^+ = (1/k)\log(k^+_{rms}) +$ const., allowing the equivalent sand roughness to be determined as $k^+_s \approx 8.2k^+_{rms}$ for case E. An empirical relationship has been derived for ΔU^+ in the transitional rough regime which includes both k^+_{rms} and ES as independent variables.

Future developments of this study could include analysing flows at higher Reynolds numbers to gain a deeper understanding of the processes involved in achieving the full roughness regime, analysing the effect of non-Gaussian surface roughness, determining the equivalent sand roughness for moderate values of ES that do not induce saturation of the roughness function and analysing non-isotropic surfaces to see the effect of different values of ES in the streamwise and spanwise directions.

Funding. This research has been supported by the European Union NextGenerationEU through the funding of the PRIN 2022 PNRR project 'SMART – Sea wave energy converters and marine tidal turbines'.

Declaration of interests. The author reports no conflict of interest.

Appendix A

This appendix contains tables with data on the rough surfaces and the results of the numerical simulations for cases A, B, C, D and E considered in this study.

Case	k_{rms}	ES	$S_{y5\times5}$	$H_{5\%5\times5}$	n_x	n_y	n_z	Δx^+	Δy^+_{min}	Δy^+_{max}	Δz^+	ΔU^+
A_1	0.005	0.018	0.018	0.013	300	220	300	10	0.57	4.76	5	0.15
A_2	0.010	0.036	0.037	0.027	300	220	300	10	0.86	4.35	5	0.45
A_3	0.020	0.072	0.074	0.053	300	250	300	10	0.84	4.5	5	1.90
A_4	0.030	0.107	0.110	0.080	300	300	300	10	0.98	3.23	5	3.55
A_5	0.040	0.143	0.149	0.107	300	300	300	10	0.98	3.94	5	5.20
A_6	0.055	0.197	0.20	0.147	300	300	300	10	1	5.21	5	7.14
A_7	0.065	0.233	0.240	0.174	300	320	300	10	1	5.05	5	8.20
A_8	0.075	0.269	0.280	0.200	300	360	300	10	1	5.55	5	9.12
A_9	0.085	0.305	0.320	0.227	300	400	300	10	0.97	4.62	5	9.98

Table 2. Rough surface parameters, set-up of the numerical simulations and ΔU^+ values for case A.

https://doi.org/10.1017/jfm.2025.61 Published online by Cambridge University Press

Case	k_{rms}	ES	$S_{y5\times5}$	$H_{5\,\%5\times5}$	n_x	n_y	n_z	Δx^+	Δy^+_{min}	Δy^+_{max}	Δz^+	ΔU^+
B_1	0.005	0.028	0.022	0.015	300	220	300	10	0.45	5.48	5	0.23
B_2	0.010	0.056	0.043	0.031	300	250	300	10	0.57	4.78	5	1.10
B_3	0.020	0.114	0.088	0.062	300	250	300	10	0.8	4.90	5	3.30
B_4	0.030	0.167	0.130	0.093	300	300	300	10	1	3.78	5	5.60
B_5	0.040	0.223	0.175	0.120	300	300	300	10	1	3.7	5	7.20
B_6	0.050	0.281	0.220	0.150	300	300	300	10	1	4.63	5	8.34
B_7	0.065	0.363	0.280	0.200	300	320	300	10	1	5.6	5	9.60
B_8	0.075	0.423	0.330	0.230	300	360	300	10	1	4.3	5	10.24
B_9	0.085	0.479	0.370	0.260	300	400	300	10	1	3.79	5	10.73

Table 3. Rough surface parameters, set-up of the numerical simulations and ΔU^+ values for case B.

Case	k_{rms}	ES	$S_{y5\times5}$	$H_{5\,\%5\times5}$	n_x	n_y	n_z	Δx^+	Δy^+_{min}	Δy^+_{max}	Δz^+	ΔU^+
C_1	0.005	0.051	0.026	0.016	360	220	300	8.33	0.68	4.5	5	0.29
C_2	0.0075	0.077	0.039	0.024	360	220	300	8.33	0.81	4.44	5	0.97
C_3	0.010	0.103	0.051	0.032	360	220	300	8.33	0.9	4.54	5	1.83
C_4	0.015	0.155	0.077	0.048	360	250	300	8.33	0.81	4.58	5	3.41
C_5	0.020	0.206	0.103	0.064	360	250	300	8.33	0.85	4.77	5	4.86
C_6	0.025	0.258	0.129	0.080	360	300	300	8.33	0.81	3.96	5	6.14
C_7	0.030	0.309	0.154	0.097	360	300	300	8.33	0.97	3.91	5	7.00
C_8	0.040	0.412	0.210	0.128	360	300	300	8.33	1	4.35	5	8.38
C_9	0.048	0.495	0.247	0.155	360	300	300	8.33	1	4.59	5	9.04
C_{10}	0.055	0.567	0.280	0.177	360	300	300	8.33	1	5.11	5	9.55
C_{11}	0.065	0.670	0.330	0.209	360	320	360	8.33	1	5.26	4.17	10.08
C_{12}	0.075	0.773	0.390	0.240	360	360	360	8.33	1	5.94	4.17	10.54
C_{13}	0.085	0.876	0.440	0.270	360	400	360	8.33	1	4.04	4.17	10.91

Table 4. Rough surface parameters, set-up of the numerical simulations and ΔU^+ values for case C.

Case	k_{rms}	ES	$S_{y5\times5}$	$H_{5\,\%5\times5}$	n_x	n_y	n_z	Δx^+	Δy^+_{min}	Δy^+_{max}	Δz^+	ΔU^+
D_1	0.005	0.067	0.028	0.016	360	220	300	8.33	0.55	2.33	5	0.8
D_2	0.010	0.134	0.057	0.032	360	220	300	8.33	0.59	5.40	5	2.63
D_3	0.020	0.278	0.114	0.065	360	250	300	8.33	0.53	6	5	5.50
D_4	0.030	0.403	0.170	0.097	360	300	300	8.33	0.97	3.90	5	7.40
D_5	0.040	0.558	0.227	0.130	360	360	300	8.33	0.8	3.68	5	8.66
D_6	0.048	0.669	0.273	0.155	360	360	300	8.33	1	2.75	5	9.30
D_7	0.055	0.767	0.313	0.178	360	360	300	8.33	0.96	3.63	5	9.70
D_8	0.065	0.906	0.370	0.210	360	360	360	8.33	1	3.67	4.17	10.20
D_9	0.075	1.030	0.426	0.240	360	360	360	8.33	1	5.94	4.17	10.62
D_{10}	0.085	1.154	0.480	0.275	360	400	360	8.33	1	5.13	4.17	10.97

Table 5. Rough surface parameters, set-up of the numerical simulations and ΔU^+ values for case D.

https://doi.org/10.1017/jfm.2025.61 Published online by Cambridge University Press

Case	k_{rms}	ES	$S_{y5\times5}$	$H_{5\%5\times5}$	n_x	n_y	n_z	Δx^+	Δy^+_{min}	Δy^+_{max}	Δz^+	ΔU^+
E_1	0.005	0.096	0.031	0.016	480	220	300	6.25	0.51	5.07	5	0.94
E_2	0.010	0.192	0.062	0.037	480	220	300	6.25	0.65	5.34	5	2.90
E_3	0.015	0.288	0.093	0.049	480	250	300	6.25	0.75	4.0	5	4.80
E_4	0.020	0.384	0.120	0.065	480	250	300	6.25	0.8	5.29	5	6.15
E_5	0.030	0.576	0.185	0.098	480	300	300	6.25	0.77	4.66	5	7.79
E_6	0.040	0.768	0.250	0.130	480	360	360	6.25	0.77	3.76	4.17	8.90
E_7	0.055	1.055	0.340	0.180	480	360	360	6.25	1	4.5	4.17	9.91
E_8	0.065	1.247	0.400	0.210	480	360	360	6.25	0.90	4.9	4.17	10.40
E_9	0.075	1.439	0.460	0.240	480	360	360	6.25	1	5.72	4.17	10.82
E_{10}	0.085	1.631	0.520	0.270	480	400	360	6.25	1	4.96	4.17	11.14

Table 6. Rough surface parameters, set-up of the numerical simulations and ΔU^+ values for case E.

References

Barros, J.M., Schultz, M.P. & Flack, K.A. 2018 Measurements of skin-friction of systematically generated surface roughness. *Intl J. Heat Fluid Flow* **72**, 1–7.

Busse, A. & Jelly, T.O. 2020 Influence of surface anisotropy of turbulent flow over irregular roughness. *Flow Turbul. Combust.* **104** (2-3), 331–354.

Busse, A. & Jelly, T.O. 2023 Effect of high skewness and kurtosis on turbulent channel flow over irregular rough walls. *J. Turbul.* **24** (1-2), 57–81.

Busse, A. & Sandham, N.D. 2012 Parametric forcing approach to rough-wall turbulent channel flow. *J. Fluid Mech.* **712**, 169–202.

Busse, A., Thakkar, M. & Sandham, N. 2017 Reynolds-number dependence of the near-wall flow over irregular rough surfaces. *J. Fluid Mech.* **810**, 196–224.

Chan, L., MacDonald, M., Chung, D., Hutchins, N. & Ooi, A. 2015 A systematic investigation of roughness height and wavelength in turbulent pipe fow in the transitionally rough regime. *J. Fluid Mech.* **771**, 743–777.

Chung, D., Hutchings, N., Schultz, M.P. & Flack, K.A. 2021 Predicting the drag of rough surfaces. *Annu. Rev. Fluid Mech.* **53** (1), 439–471.

De Marchis, M., Saccone, D., Milici, B. & Napoli, E. 2020 Large eddy simulations of rough turbulent channel flows bounded by irregular roughness: advances toward a universal roughness correlation. *Turbul. Combust.* **105** (2), 627–648.

Dunbar, D., Van Der A., D.A., Scandura, P., & O'Donoghue, T. 2023 An experimental and numerical study of turbulent oscillatory flow over an irregular rough wall. *J. Fluid Mech.* **955**, 47.

Flack, K.A. & Schultz, M.P. 2010 Review of hydraulic roughness scales in the fully rough regime. *J. Fluids Engng ASCE* **132** (4), 10.

Flack, K.A., Schultz, M.P. & Barros, J.M. 2020 Skin friction measurements of systematically-varied roughness: probing the role of roughness amplitude and skewness. *Flow Turbul. Combust.* **104** (2-3), 317–329.

Forooghi, P., Frohnapfel, B., Magagnato, F. & Busse, A. 2018 A modified parametric forcing approach for modelling of roughness. *Intl J. Heat Fluid Flow* **71**, 200–209.

Forooghi, P., Stroh, A., Magagnato, F., Jakirlic, S. & Frohnapfel, B. 2017 Toward a universal roughness correlation. *J. Fluids Engng* **139** (12), 12.

Guo-Zhen, M., Chun-Xiao, X., Hyung, J.S. & Wei-Xi, H. 2020 Scaling of rough-wall turbulence by the roughness height and steepness. *J. Fluid Mech.* **900**, 13.

Jelly, T.O., Ramani, A., Nugroho, B., Hutchins, N. & Busse, A. 2022 Impact of spanwise effective slope upon rough-wall turbulent channel flow. *J. Fluid Mech.* **951**, A1.

Jiménez, J. 2004 Turbulent flows over rough walls. *Annu. Rev. Fluid Mech.* **36** (1), 173–196.

Kuwata, Y. & Nagura, R. 2020 Direct numerical simulation on the effects of surface slope and skewness on roughwall turbulence. *Phys. Fluids* **32** (105113) 350–365.

Leonardi, S., Orlandi, P., Smalley, R.J., Djenidi, L., Paden, J.D. & Antonia, R.A. 2003 Direct numerical simulations of turbulent channel flow with transverse square bars on one wall. *J. Fluid Mech.* **491**, 229–238.

https://doi.org/10.1017/jfm.2025.61 Published online by Cambridge University Press

MA, R., ALAMÉ, K. & MAHESH, K. 2021 Direct numerical simulation of turbulent channel flow over random rough surfaces. *J. Fluid Mech.* **908**, A40.

MACDONALD, M., CHAN, L., CHUNG, D., HUTCHINGS, N. & OOI, A. 2016 Turbulent fow over transitionally rough surfaces with varying roughness densities. *J. Fluid Mech.* **804**, 130–161.

MEAKIN, P. 1998 *Fractals, Scaling and Growth Far From Equilibrium*. Cambridge University Press.

NAPOLI, E., ARMENIO, V. & DE MARCHIS, M. 2008 The effect of the slope of irregularly distributed roughness elements on turbulent wall-bounded flows. *J. Fluid Mech.* **613**, 385–394.

NIKORA, V.I., GORING, D.G. & BIGGS, B.J.F. 1998 On gravel-bed roughness characterization. *Water Resour. Res.* **34** (3), 517–527.

NIKURADSE, J. 1933 Stromungsgesetze in rauhen rohren. Forschung auf dem Gebiete des Ingenieurwesens, Forschungsheft 361. VDI Verlag, Berlin, Germany. (in German) (English translation: Laws of flow in rough pipes, NACA TM 1292, 1950).

OROSEI, R., BIANCHI, R., CORADINI, A., ESPINASSE, S., FEDERICO, C., FERRICIONI, A. & GAVRISHIN, A.I. 2003 Self-affine behaviour of martian topography at kilometer scale from Mars orbiter laser. *J. Geophys. Res.* **108** (E4), 8023.

PONSON, I., BONAMY, D., AURADOU, H., MOUROT, G., MOREL, S., BOUCHAUD, E., GUILLOT, C. & HULIN, J.P. 2006 Anisotropic self-affine properties of experimental fracture surfaces. *Intl J. Fracture* **140** (1-4), 27–37.

PORTELA, F.A., BUSSE, A. & SANDHAM, N.D. 2021 Numerical study of Fourier-filtered rough surfaces. *Phys. Rev. Fluids* **6**, 27.

RAMANI, T.O., SCHILT, L., NUGROHO, B., BUSSE, A. & JELLY, T.O. 2024 An assessment of effective slope as a parameter for turbulent drag prediction over multi-scaled roughness. *Exp. Fluids* **65** (6), 1–15.

SCHLICHTING, H. 1936 Experimentelle untersuchungen zum rauhigkeitsproblem. *Ing.-Arch.* **7** (1), 1–34. See also: Experimental investigation of the problem of surface roughness. Translation from German published 1937 as NACA Tech. Memo. 823.

SCHULTZ, M.P. & FLACK, K.A. 2009 Turbulent boundary layers on a systematically varied rough wall. *Phys. Fluids* **21** (1), 015104.

STEWART, M.T., STUART, M.C., NIKORA, V.I., ZAMPIRON, A. & MARUSIC, I. 2019 Hydraulic resistance in open-channel flows over self affine rough beds. *J. Hydraul. Res.* **57** (2), 183–196.

THAKKAR, M., BUSSE, A. & SANDHAM, N. 2017 Surface correlations of hydrodynamic drag for transitionally rough engineering surfaces. *J. Turbul.* **18** (2), 138–169.

THAKKAR, M., BUSSE, A. & SANDHAM, N.D. 2018 Direct numerical simulation of turbulent channel flow over a surrogate for Nikuradse-type roughness. *J. Fluid Mech.* **837**, R1.

TURCOTTE, D.L. 1997 *Fractal and Chaos in Geology and Geophysics*. Cambridge University Press.

VAN RIJN, L.C. 1982 Equivalent roughness of alluvial bed. *J. Hydraul Div. ASCE* **108** (10), 1215–1218.

WHITING, P.J. & DIETRICH, W.E. 1990 Boundary shear stress and roughness over mobile alluvial beds. *J. Hydraul. Engng ASCE* **116** (12), 1495–1511.

YANG, J., STROH, A., CHUNG, D. & FOROOGHI, P. 2022 Direct numerical simulation-based characterization of pseudo-random roughness in minimal channels. *J. Fluid Mech.* **941**, A7.

YANG, J., STROH, A., LEE, S., BAGHERI, S., FROHNAPFEL, B. & FOROOGHI, P. 2023*a* Prediction of equivalent sand-grain size and identification of drag-relevant scales of roughness – a data–driven approach. *J. Fluid Mech.* **975**, 7.

YANG, X.I.A., ZHANG, W., YUAN, J. & KUNZ, R.F. 2023*b* In search of a universal rough wall model. *J. Fluids Engng* **145** (10), 7.

YUAN, J. & PIOMELLI, U. 2014*a* Estimation and prediction of the roughness function on realistic surfaces. *J. Turbul.* **15** (6), 350–365.

YUAN, J. & PIOMELLI, U. 2014*b* Roughness effects on the Reynolds stress budgets in near-wall turbulence. *J. Fluid Mech.* **760**, R1.

https://doi.org/10.1017/jfm.2025.61 Published online by Cambridge University Press